

Anisotropic yield function of hexagonal materials taking into account texture development and anisotropic hardening

B. Plunkett^a, R.A. Lebensohn^b, O. Cazacu^{a,*}, F. Barlat^c

^a Department of Mechanical and Aerospace Engineering, University of Florida/REEF, 1350 N Poquito Road, Shalimar, FL 32579-1163, USA

^b Los Alamos National Laboratory, MST8, MS G755, Los Alamos, NM 87545, USA

^c Materials Science Division, Alcoa Inc., Alcoa Technical Center, 100 Technical Drive, Alcoa Center, PA 15069-0001, USA

Received 13 October 2005; received in revised form 4 May 2006; accepted 4 May 2006

Available online 1 August 2006

Abstract

Because of twinning and texture evolution, the yield surface for hexagonal close-packed (hcp) metals significantly changes its shape with accumulated plastic deformation. Traditional hardening laws cannot accurately model these phenomena. In this paper, an anisotropic model that captures the influence of evolving texture on the plastic response of hcp metals is proposed. Initial yielding is described using a recently developed analytical yield function that accounts for both anisotropy and strength differential effects. To describe the change of the shape of the yield surface during monotonic loading, the evolution of the anisotropic coefficients involved in the expression of the yield function is considered. The evolution laws for the anisotropic coefficients are obtained based on experimental data and crystal plasticity theory, together with a macroscopic-scale interpolation technique. This approach is further applied to the description of the mechanical behavior of high-purity zirconium at room temperature. Validation of the proposed model is provided by applying it to the simulation of the three-dimensional deformation of a beam subjected to four-point bending along different directions with respect to the hard-to-deform $\langle c \rangle$ -axis predominant orientation of the material. Comparison between predicted and measured macroscopic strain fields and beam sections shows that the proposed model describes very well the difference in response between the tensile and compressive fibers and the shift of the neutral axis.

© 2006 Acta Materialia Inc. Published by Elsevier Ltd. All rights reserved.

Keywords: Twinning; Texture evolution; Yielding asymmetry; Anisotropic yielding; Zirconium

1. Introduction

Characterization of the plastic response in metals requires the specification of a yield function and a flow rule by which subsequent inelastic deformation can be calculated for specified loadings and displacements. Traditionally, the evolution of the yield surface is described by a combination of isotropic and kinematic hardening laws. Isotropic hardening implies a proportional expansion of the surface, without any changes in shape or position. An isotropic hardening model is only truly valid for monotonic

loading along a given strain path assuming that every strain path hardens at the same rate. For simulation of sheet forming operations of cubic metals (both face-centered cubic (fcc) and body-centered cubic (bcc)), such an assumption is reasonably adequate [1]. Pure translation of the initial yield surface could be described by the classic linear kinematic hardening laws [2,3]. To model more accurately the smooth elastic–plastic transition upon reverse loading, multi-surface models as well as nonlinear kinematic hardening models have been proposed. Reviews of such models may be found in Refs. [4–6].

Because of non-negligible twinning activity accompanied by grain reorientation and highly directional grain interactions, the influence of the texture evolution on hardening of hexagonal close-packed (hcp) materials cannot be

* Corresponding author. Tel.: +1 850 833 9350; fax: 1 850 833 9366.
E-mail address: cazacu@gerc.eng.ufl.edu (O. Cazacu).

neglected even for the simplest monotonic loading paths. To describe with accuracy the evolution of yield loci it is imperative to account for the most important sources of anisotropy in the given material: slip and/or twinning activity, substructure evolution at grain level and texture development during deformation. Since in crystal plasticity models (see e.g. Refs. [7,8]) the distribution of crystal orientations in the given polycrystal, the available slip/twinning deformation systems and the stress levels necessary to activate them are taken into account explicitly, the evolution of anisotropy due to texture development can be characterized by measuring the initial texture and calculating the grain reorientation (i.e. updating the texture) using a suitable homogenization scheme (e.g. a Taylor model or a self-consistent model). Recently, the application of crystal plasticity models to hcp metals and the incorporation of crystal plasticity calculations directly into finite element (FE) analyses have received much attention. Models that account for both slip and twinning activity and employ Taylor [9–11] or self-consistent [12,13] averaging schemes to predict the aggregate behavior have been proposed. For example, the model of Staroselsky and Anand [10] neglects hardening but accounts for the intragranular effects on plastic deformation observed in magnesium alloys. Salem et al. [11] concentrated their attention on the characterization of the strain-hardening behavior of high-purity titanium during compression at room temperature and the development of slip-hardening and twin-hardening functions. These laws were incorporated into a Taylor crystal plasticity framework and further used to simulate the stress–strain response and texture evolution for monotonic loading (uniaxial compression and simple shear). However, no attempt was made to predict the final deformed shape of the specimens, nor to perform benchmark simulations of more complex monotonic loadings such as bending. In Refs. [12,13], a self-consistent viscoplastic model linked to the explicit FE code EPIC has been successfully used for describing the deformation of pure zirconium with a strong initial texture under quasi-static monotonic loading at room and liquid nitrogen temperatures.

The above direct implementations of polycrystal models into FE codes, where a polycrystalline aggregate is associated with each FE integration point, have the advantage that they follow the evolution of anisotropy due to texture development. However, such FE calculations are computationally very intensive, thus limiting the applicability of these approaches to problems that do not require a fine spatial resolution. An alternative approach is to develop anisotropic formulations at a macroscopic level that can be easily implemented in FE codes, and thus can be applied routinely for detailed analyses of complex forming processes. Methods to determine analytical expressions for the plastic potential in the strain rate space based on texture data have been proposed by Arminjon et al. [14] and Van Houtte and collaborators (e.g. Ref. [15]). The coefficients of an adjustable plastic

potential (up to several hundreds of them) are obtained by minimizing the difference between the plastic work rate computed using such plastic potential and the plastic work rate computed using crystal plasticity for a large number of strain modes. This approach, in conjunction with the Taylor model and isotropic hardening, has been implemented in FE codes and applied to the modeling of texture-induced anisotropy of sheet forming of fcc and bcc materials (see e.g. Ref. [16]). Also recently, a complex constitutive model that couples a texture-adjusted anisotropic plastic potential with a physically based hardening model involving several tensorial variables has been proposed [17,18]. It has been shown that the model captures very well the microstructure evolution under arbitrary strain-path changes in low-carbon steels. However, the model neglects texture evolution during plastic deformation [18]. It is to be noted that no attempt to use the aforementioned texture-based approaches for the determination of analytic expressions of the plastic potential of hcp materials has been reported.

Unlike recent progress in the development of mathematical descriptions of anisotropic yield surfaces for materials with cubic structure [19–23], phenomenological modeling of hcp materials is less developed. Due to the lack of adequate macroscopic yield criteria for hcp materials, hcp sheet forming FE simulations are still performed using classic anisotropic formulations for cubic metals such as Hill's 1948 criterion [24] (see e.g. Refs. [25,26]). Some of the rigorous methods proposed to account for initial plastic anisotropy or to describe an average material response over a certain deformation range [20,23] can be extended to hcp materials. The major difficulty encountered in formulating analytic expressions for the yield functions of hcp metals is related to the description of the strength differential effect (tension vs. compression asymmetry due to twinning). Recently, yield functions in the full stress space which capture both the tension/compression asymmetry and the anisotropic behavior of hcp metals and alloys were developed [27,28]. In particular, the capability of the Cazacu–Plunkett–Barlat 2005 yield criterion [28] (further denoted as CPB05) to describe accurately the shape of yield surfaces corresponding to individual equivalent plastic deformation levels of textured polycrystalline binary Mg–Th and Mg–Li alloys (data after Kelley and Hosford [29]) was demonstrated in Ref. [28].

The objective of the present paper is to propose a macroscopic model that captures the evolution of anisotropy due to evolving texture in hexagonal metals subjected to monotonic loading conditions. Yielding is described using the CPB05 yield criterion. To model the change in shape of the yield locus during plastic deformation, evolution laws for the anisotropic coefficients involved in the expression of the CPB05 yield function are determined using a macroscopic-scale interpolation technique and experimental data. For the strain paths for which experimental data were not available, flow stress data were calculated with a viscoplastic self-consistent model. This approach is further

applied to the description of the mechanical behavior of high-purity zirconium at room temperature.

2. Polycrystal model

Characterization of the effect of evolving crystallographic texture on the plastic response of hexagonal materials by direct mechanical testing is a challenging task even for simple loading conditions. To generate information concerning the evolution of the yield loci with accumulated deformation, we performed numerical tests using the viscoplastic self-consistent (VPSC) model [30]. While this formulation is briefly reviewed in what follows, a detailed description can be found in the review article by Tomé and Lebensohn [8]. The polycrystal is represented by a finite set of orientations, each one representing a given volume fraction chosen to reproduce the initial texture. The total deformation of the polycrystal is achieved by imposing successive strain increments and calculating the resulting shears in the active deformation (slip and/or twinning) systems in the grains. The final texture is given by the grain reorientations associated with these shears. A self-consistent approach is used to model the interaction of a grain with the surroundings. Each grain is treated as an anisotropic, viscoplastic, ellipsoidal inclusion embedded in a uniform matrix having the unknown properties (to be determined) of the polycrystal. Elastic deformations are neglected. Each deformation system (s) is characterized by a vector \mathbf{n}^s (normal to the slip or twinning plane) and a vector \mathbf{b}^s (Burgers vector or twinning shear direction). The local constitutive behavior (at the grain level) is described by

$$\dot{\boldsymbol{\varepsilon}}^g = \sum_s \mathbf{m}^s \dot{\gamma}^s = \dot{\gamma}_0 \sum_s \mathbf{m}^s \left(\frac{\mathbf{m}^s : \boldsymbol{\sigma}^g}{\tau_c^s} \right)^n, \quad (1)$$

where $\mathbf{m}^s = \frac{1}{2}(\mathbf{b}^s \otimes \mathbf{n}^s + \mathbf{n}^s \otimes \mathbf{b}^s)$, $\dot{\gamma}^s$ and τ_c^s are, respectively, the Schmid tensor, the shear rate and the critical stress of system (s), $\dot{\boldsymbol{\varepsilon}}^g$ and $\boldsymbol{\sigma}^g$ are the local averages of the strain rate and stress fields in grain (g), $\dot{\gamma}_0$ is a reference shear rate and n is a rate sensitivity parameter. Eq. (1) expresses that the deformation rate is given by the sum over all the shear rates contributed by all systems. The activation criterion (both for slip and twinning) is given by the expression in parenthesis: the activity on each deformation system (s) increases when the resolved shear on that system (given by $\mathbf{m}^s : \boldsymbol{\sigma}^g$) approaches a threshold value τ_c^s . However, twinning differs from slip in its directionality, i.e. it can be only activated by a positive shear. Strain-hardening is incorporated by allowing the critical stress τ_c^s to increase in an interval Δt according to

$$\tau_c^s = \tau_0^s + (\tau_1^s + \theta_1^s \Gamma^s) \left(1 - \left(\frac{\theta_0^s \Gamma^s}{\tau_1^s} \right) \right), \quad (2)$$

where τ_0^s , τ_1^s , θ_0^s and θ_1^s are constants, and $\Gamma^s = \sum_s \dot{\gamma}^s \Delta t$ is the accumulated shear in all deformation systems. The nonlinear expression equation (1) can be linearized using a tangent approximation:

$$\dot{\boldsymbol{\varepsilon}}^g \cong \mathbf{M}^{\text{tg}}(\boldsymbol{\sigma}^g) : \boldsymbol{\sigma}^g + \dot{\boldsymbol{\varepsilon}}_0^g(\boldsymbol{\sigma}^g) \quad (3)$$

with

$$\mathbf{M}^{\text{tg}} = n \dot{\gamma}_0 \sum_s \frac{\mathbf{m}^s \otimes \mathbf{m}^s}{\tau_c^s} \left(\frac{\mathbf{m}^s : \boldsymbol{\sigma}^g}{\tau_c^s} \right)^{n-1} \quad (4)$$

$$\text{and } \dot{\boldsymbol{\varepsilon}}_0^g = (1 - n) \dot{\boldsymbol{\varepsilon}}^g.$$

At the macroscopic level, the overall response of the polycrystal can also be assumed to be described by a tangent relation:

$$\dot{\boldsymbol{\varepsilon}} = \bar{\mathbf{M}}^{\text{tg}} : \bar{\boldsymbol{\sigma}} + \dot{\boldsymbol{\varepsilon}}^0, \quad (5)$$

where $\dot{\boldsymbol{\varepsilon}}$ and $\bar{\boldsymbol{\sigma}}$ are the effective strain rate and stress, respectively, $\bar{\mathbf{M}}^{\text{tg}}$ is the macroscopic tangent compliance moduli and $\dot{\boldsymbol{\varepsilon}}^0$ is the back-extrapolated macroscopic strain rate. As previously mentioned, the interaction of the grain with its surroundings is accounted for by assuming each grain to be an inclusion embedded in an infinite homogeneous matrix having the overall properties of the polycrystal. The following interaction equation results:

$$(\dot{\boldsymbol{\varepsilon}}^g - \dot{\boldsymbol{\varepsilon}}) = -\tilde{\mathbf{M}} : (\boldsymbol{\sigma}^g - \bar{\boldsymbol{\sigma}}), \quad (6)$$

where

$$\tilde{\mathbf{M}} = (\mathbf{I} - \mathbf{S}_E)^{-1} : \mathbf{S}_E : \bar{\mathbf{M}}^{\text{tg}}. \quad (7)$$

In Eq. (7), \mathbf{S}_E is the viscoplastic Eshelby tensor, a function of the properties of the effective medium (i.e. $\bar{\mathbf{M}}^{\text{tg}}$) and the inclusion (grain) shape [31]. The self-consistent equation, which allows adjustment of the macroscopic compliance by requiring a matching between the overall averages of the local fields and the corresponding effective magnitudes, reads

$$\bar{\mathbf{M}}^{\text{tg}} = \langle \mathbf{M}^{\text{tg}} : \mathbf{B}^g \rangle, \quad (8)$$

where $\langle \cdot \rangle$ denotes average over the set of grains that represents the polycrystal, and where the localization tensor \mathbf{B}^g (that links the local and effective stresses, i.e. $\boldsymbol{\sigma}^g = \mathbf{B}^g : \bar{\boldsymbol{\sigma}}$) is given by

$$\mathbf{B}^g = \left(\frac{1}{n} \mathbf{M}^{\text{tg}} + \tilde{\mathbf{M}} \right)^{-1} : \left(\frac{1}{n} \bar{\mathbf{M}}^{\text{tg}} + \tilde{\mathbf{M}} \right). \quad (9)$$

Once $\bar{\mathbf{M}}^{\text{tg}}$ is adjusted by means of Eq. (9), Eqs. (1), (6) and (7) can be combined into a system of nonlinear equations to solve for the local stress and strain rate in each grain.

Finally, it should be mentioned that the twinning contribution to texture development is accounted for by means of the so-called predominant twin reorientation (PTR) scheme, which essentially consists of determining the grains where twinning is most active and reorienting them completely into the orientation of their most active twinning system, accounting in this way for the volumetric effect of twinning reorientation on texture development and at the same time maintaining fixed the number of orientations that represent the polycrystal (see Ref. [31] for details).

3. Proposed macroscopic model

3.1. Initial yielding

In order to develop a macroscopic elastoplastic model to capture the evolution of anisotropy due to evolving texture in hexagonal metals subjected to monotonic loading conditions, yielding is described here by means of the CPB05 criterion [28] that accounts for both anisotropy and asymmetry in yielding between tension and compression. The CPB05 criterion is an extension to orthotropy of an isotropic yield criterion of the form

$$f(\mathbf{S}) = (|S_1| - kS_1)^a + (|S_2| - kS_2)^a + (|S_3| - kS_3)^a, \quad (10)$$

where S_i , $i = 1, \dots, 3$, are the principal values of \mathbf{S} , the deviator of the Cauchy stress $\boldsymbol{\sigma}$; the coefficient k allows for the description of strength differential effects; and the integer a is the degree of homogeneity. Specifically, for a fixed value of the parameter a , the parameter k can be expressed solely in terms of the ratio between σ_T , the uniaxial yield in tension, and σ_C the uniaxial yield in compression, respectively:

$$k = \frac{1 - \left\{ \frac{2^a - 2 \cdot (\sigma_T / \sigma_C)^a}{(2 \cdot \sigma_T / \sigma_C)^a - 2} \right\}^{\frac{1}{a}}}{1 + \left\{ \frac{2^a - 2 \cdot (\sigma_T / \sigma_C)^a}{(2 \cdot \sigma_T / \sigma_C)^a - 2} \right\}^{\frac{1}{a}}}. \quad (11)$$

Note that for $a = 2$ and $k = 0$, which corresponds to equal yield stresses in tension and compression, the Von Mises yield criterion is recovered.

The isotropic criterion (Eq. (10)) was extended to orthotropy by using a linear transformation on the deviatoric stress tensor, i.e. in Eq. (10), S_1 , S_2 , S_3 are substituted by the principal values of a transformed tensor $\boldsymbol{\Sigma}$ defined as

$$\boldsymbol{\Sigma} = \mathbf{L} : \mathbf{S}. \quad (12)$$

Thus, the anisotropic yield criterion CPB05 is of the form

$$F = (|\Sigma_1| - k\Sigma_1)^a + (|\Sigma_2| - k\Sigma_2)^a + (|\Sigma_3| - k\Sigma_3)^a, \quad (13)$$

where $\Sigma_1, \Sigma_2, \Sigma_3$ are the principal values of $\boldsymbol{\Sigma}$. The only restrictions imposed on the fourth-order tensor \mathbf{L} are: (i) to satisfy the major and minor symmetries and (ii) to be invariant with respect to the orthotropy group. Thus, for three-dimensional stress conditions CPB05 involves nine independent anisotropy coefficients and it reduces to the isotropic criterion of Eq. (9) when \mathbf{L} is equal to the fourth-order identity tensor. It is worth noting that although the transformed tensor is not deviatoric, the orthotropic criterion is insensitive to hydrostatic pressure and thus the condition of plastic incompressibility is satisfied (see Ref. [28] for details). For $k \in [-1, 1]$ and any integer $a \geq 1$, the anisotropic yield function is convex in the variables $\Sigma_1, \Sigma_2, \Sigma_3$.

Identification of the material parameters involved in the above yield criterion for an orthotropic sheet can be done using (i) experimental yield stress values corresponding to monotonic uniaxial tension and compression along different directions in the plane of the sheet and through-thickness

compression, and (ii) r -values along the rolling and transverse directions obtained from uniaxial tension and compression tests, respectively (for more details, see Ref. [28]).

It was shown that this criterion is able to reproduce individual plane stress yield surfaces corresponding to different given (fixed) levels of accumulated plastic deformation for pure Mg as well as for Mg and Ti alloys (see Ref. [28], data after Ref. [32]). However, modeling the change in the shape of the yield locus which is due to texture evolution during plastic deformation is a daunting task, even for monotonic loading conditions. In this work we focus on the description of the evolution of anisotropy for such monotonic strain paths (i.e. anisotropic hardening effects associated to strain-path changes like the Bauschinger effect will not be considered).

We assume that yielding is described by:

$$F(\boldsymbol{\sigma}, \tilde{\epsilon}_p) = \tilde{\sigma}(\boldsymbol{\sigma}, \tilde{\epsilon}_p) - Y(\tilde{\epsilon}_p). \quad (14)$$

In Eq. (14), $\tilde{\sigma}$ is the effective stress based on the stress potential given by Eq. (13) i.e.

$$\tilde{\sigma} = B [(|\Sigma_1| - k\Sigma_1)^a + (|\Sigma_2| - k\Sigma_2)^a + (|\Sigma_3| - k\Sigma_3)^a]^{\frac{1}{a}}, \quad (15)$$

where B is a constant defined such that $\tilde{\sigma}$ reduces to the tensile yield stress in the rolling direction, i.e.

$$B = \left[\frac{1}{(|\Phi_1| - k\Phi_1)^a + (|\Phi_2| - k\Phi_2)^a + (|\Phi_3| - k\Phi_3)^a} \right]^{\frac{1}{a}} \quad (16)$$

with

$$\begin{aligned} \Phi_1 &= \left(\frac{2}{3}L_{11} - \frac{1}{3}L_{12} - \frac{1}{3}L_{13} \right), \\ \Phi_2 &= \left(\frac{2}{3}L_{12} - \frac{1}{3}L_{22} - \frac{1}{3}L_{23} \right), \\ \Phi_3 &= \left(\frac{2}{3}L_{13} - \frac{1}{3}L_{23} - \frac{1}{3}L_{33} \right) \end{aligned} \quad (17)$$

and where $Y(\tilde{\epsilon}_p)$ is the isotropic hardening law in which $\tilde{\epsilon}_p$ is the effective plastic strain. The effective plastic strain associated with this anisotropic yield function is calculated using the principle of equivalence of plastic work (see Ref. [33]).

Note that even if, for a given level of strain, the components of the fourth-order tensor \mathbf{L} and the coefficients k and a can be determined based on the available experimental data, establishing analytical expressions for the evolution of all these parameters in terms of the hardening variable is very challenging. Therefore, an alternative approach is proposed.

3.2. Evolution of the yield surface with accumulated deformation

The methodology proposed is to complement available experimental data with numerical test results. For this purpose, we use the VPSC model to calculate the yield stresses

along strain paths for which no experimental data are available. Since the polycrystalline model incorporates explicitly the evolution of texture, we can thus obtain information concerning the change of the shape of the yield locus with accumulated deformation. Using this combination of experimental and numerical results, we then identify the coefficients involved in the CPB05 yield criterion for a finite set of values of equivalent plastic strain, say $\tilde{\epsilon}_p^1 < \tilde{\epsilon}_p^2 < \dots < \tilde{\epsilon}_p^m$, and then calculate the effective stress $\tilde{\sigma}^j = \tilde{\sigma}\{\boldsymbol{\sigma}, \mathbf{L}(\tilde{\epsilon}_p^j), k(\tilde{\epsilon}_p^j), a(\tilde{\epsilon}_p^j)\}$ (according to Eq. (15)) as well as $Y^j = Y(\tilde{\epsilon}_p^j)$, corresponding to the each of the individual strain levels $\tilde{\epsilon}_p^j, j = 1, \dots, m$. Further, an interpolation procedure is used to obtain the yield surfaces corresponding to any given level of accumulated strain. For a given arbitrary $\tilde{\epsilon}_p$, the anisotropic yield function is of the form

$$F(\boldsymbol{\sigma}, \tilde{\epsilon}_p) = \Gamma(\boldsymbol{\sigma}, \tilde{\epsilon}_p) - \Pi(\tilde{\epsilon}_p) \quad (18)$$

with

$$\Gamma = \xi(\tilde{\epsilon}_p) \cdot \tilde{\sigma}^j + (1 - \xi(\tilde{\epsilon}_p)) \cdot \tilde{\sigma}^{j+1} \quad (19)$$

and

$$\Pi = \xi(\tilde{\epsilon}_p) \cdot Y^j + (1 - \xi(\tilde{\epsilon}_p)) \cdot Y^{j+1} \quad (20)$$

for any $\tilde{\epsilon}_p^j \leq \tilde{\epsilon}_p \leq \tilde{\epsilon}_p^{j+1}, j = 1, \dots, m - 1$. For linear interpolation, the weighting parameter $\xi(\tilde{\epsilon}_p)$ appearing in Eqs. (19) and (20) is defined as

$$\xi(\tilde{\epsilon}_p) = \frac{\tilde{\epsilon}_p^{j+1} - \tilde{\epsilon}_p}{\tilde{\epsilon}_p^{j+1} - \tilde{\epsilon}_p^j} \quad (21)$$

such that $\xi(\tilde{\epsilon}_p^j) = 1$ and $\xi(\tilde{\epsilon}_p^{j+1}) = 0$. By considering that the anisotropy coefficients L_{ij} , the strength differential parameter k and the homogeneity parameter a evolve with the plastic deformation, the observed distortion and change in shape of the yield loci of hcp materials can be captured. Obviously, if these coefficients are taken constant, then the shape of the yield locus depends only on the initial texture and does not change.

3.3. Integration algorithm

In order to simulate the deformation of hcp metals the proposed model was implemented in the commercial FE code ABAQUS [34]. The algorithmic aspects related to the FE implementation are presented in what follows. The elastic strains are usually much smaller than the plastic strains, and hence an additive decomposition of the total strain rate $\dot{\boldsymbol{\epsilon}}$ into an elastic part $\dot{\boldsymbol{\epsilon}}^e$ and a plastic part $\dot{\boldsymbol{\epsilon}}^p$ is usually considered. Thus, the constitutive equations can be written in a rate form as

$$\dot{\boldsymbol{\epsilon}} = \dot{\boldsymbol{\epsilon}}^e + \dot{\boldsymbol{\epsilon}}^p. \quad (22)$$

The elastic stress–strain relationship is given by

$$\dot{\boldsymbol{\sigma}} = \mathbf{C} : \dot{\boldsymbol{\epsilon}}^e, \quad (23)$$

where \mathbf{C} denotes the fourth-order elasticity tensor. The yield function is given by Eq. (18) and the evolution of the plastic strain is given by an associated flow rule:

$$\dot{\boldsymbol{\epsilon}}^p = \lambda \frac{\partial F}{\partial \boldsymbol{\sigma}}, \quad (24)$$

where $\lambda \geq 0$ is the plastic multiplier. Since the effective stress $\tilde{\sigma}$ is a first-order homogeneous function in stresses (see Eq. (15)), from the work-equivalence principle it follows that the law of evolution for the effective plastic strain (associated with $\tilde{\sigma}$) reduces to $\dot{\tilde{\epsilon}}^p = \lambda$. The loading–unloading conditions can be expressed in Kuhn–Tucker form as $\lambda \geq 0, F \leq 0, \lambda F = 0$.

$$(25)$$

Using the preceding relationships, it can be easily shown that the tensor of tangent elastoplastic moduli, \mathbf{C}^{ep} , which relates the current stress increment to the current total strain increment, is given by

$$\mathbf{C}^{ep} = \begin{cases} \mathbf{C} & \text{if } \lambda = 0, \\ \mathbf{C} - \frac{\mathbf{C} \frac{\partial \Gamma}{\partial \boldsymbol{\sigma}} \otimes \mathbf{C} \frac{\partial \Gamma}{\partial \boldsymbol{\sigma}}}{\frac{\partial \Gamma}{\partial \boldsymbol{\sigma}} \cdot \mathbf{C} \frac{\partial \Gamma}{\partial \boldsymbol{\sigma}} - \frac{\partial \Pi}{\partial \tilde{\epsilon}_p} \frac{\partial \Gamma}{\partial \tilde{\epsilon}_p}} & \text{if } \lambda > 0, \end{cases} \quad (26)$$

where

$$\frac{\partial \Gamma}{\partial \boldsymbol{\sigma}} = \xi(\tilde{\epsilon}_p) \cdot \frac{\partial \tilde{\sigma}^j}{\partial \boldsymbol{\sigma}} + (1 - \xi(\tilde{\epsilon}_p)) \cdot \frac{\partial \tilde{\sigma}^{j+1}}{\partial \boldsymbol{\sigma}}, \quad (27)$$

$$\frac{\partial \Gamma}{\partial \tilde{\epsilon}_p} = \frac{\tilde{\sigma}^{j+1} - \tilde{\sigma}^j}{\tilde{\epsilon}_p^{j+1} - \tilde{\epsilon}_p^j}, \quad (28)$$

$$\frac{\partial \Pi}{\partial \tilde{\epsilon}_p} = \frac{Y^{j+1} - Y^j}{\tilde{\epsilon}_p^{j+1} - \tilde{\epsilon}_p^j}. \quad (29)$$

In order to solve for the plastic multiplier, the following second derivatives of the yield function are also generally necessary:

$$\frac{\partial^2 \Gamma}{\partial \boldsymbol{\sigma}^2} = \xi(\tilde{\epsilon}_p) \frac{\partial^2 \tilde{\sigma}^j}{\partial \boldsymbol{\sigma}^2} + (1 - \xi(\tilde{\epsilon}_p)) \frac{\partial^2 \tilde{\sigma}^{j+1}}{\partial \boldsymbol{\sigma}^2}, \quad (30)$$

$$\frac{\partial^2 \Gamma}{\partial \tilde{\epsilon}_p \partial \boldsymbol{\sigma}} = \frac{\frac{\partial \Gamma^{j+1}}{\partial \boldsymbol{\sigma}} - \frac{\partial \Gamma^j}{\partial \boldsymbol{\sigma}}}{\tilde{\epsilon}_p^{j+1} - \tilde{\epsilon}_p^j}. \quad (31)$$

In displacement-based FE formulations, for a prescribed nodal displacement, at each Gauss point the system of Eqs. (22)–(24) is integrated to update stress and hardening parameter. As integration algorithm we used the closest point projection algorithm (see e.g. Refs. [35,36]). During a time step $[t_n, t_{n+1}]$, the trial stress $\boldsymbol{\sigma}_{n+1}^{\text{trial}} = \boldsymbol{\sigma}_n + \mathbf{C} : \Delta \boldsymbol{\epsilon}_n$ is calculated.

If $F(\boldsymbol{\sigma}_{n+1}^{\text{trial}}, \tilde{\epsilon}_n^p) \leq 0$, $\boldsymbol{\sigma}_{n+1} = \boldsymbol{\sigma}_{n+1}^{\text{trial}}$, if $F(\boldsymbol{\sigma}_{n+1}^{\text{trial}}, \tilde{\epsilon}_n^p) - \Pi(\tilde{\epsilon}_n^p) > 0$, there is plastic flow, and integration of the constitutive equation leads to the following nonlinear system:

$$\boldsymbol{\sigma}_{n+1} = \boldsymbol{\sigma}_{n+1}^{\text{trial}} - \Delta \lambda \mathbf{C} : \left(\frac{\partial F}{\partial \boldsymbol{\sigma}} \right)_{n+1}, \quad (32)$$

$$F_{n+1} = \Gamma(\boldsymbol{\sigma}_{n+1}, \tilde{\epsilon}_n^p + \Delta \lambda) - \Pi(\tilde{\epsilon}_n^p + \Delta \lambda) = 0$$

to be solved for $\boldsymbol{\sigma}_{n+1}$ and $\Delta \lambda$. The integration of Eq. (32) is performed iteratively, starting with $\boldsymbol{\sigma}_{n+1}^0 = \boldsymbol{\sigma}_{n+1}^{\text{trial}}$ and $\Delta \lambda^{(0)} = 0$. Then, given $\boldsymbol{\sigma}_n^{(k)}$ and $\tilde{\epsilon}_n^{p(k)}$, an iterative procedure is performed. Basically, the constraint equation (32) is linearized and the increment to the plastic multiplier is computed. The stresses and strains are then updated through λ^{n+1} , and the yield criterion $F(\boldsymbol{\sigma}_{n+1}, \tilde{\epsilon}_p) \leq 0$ should

be satisfied within a specified tolerance. If this tolerance has not been met, then the plastic corrector step will be repeated until convergence is obtained. Once this happens, the updated stresses and strains are accepted as the current state.

In what follows, the proposed model will be applied to the description of the quasi-static behavior of high-purity zirconium at room temperature (data reported in Refs. [12,13,37]) during in-plane tension, in-plane compression and bending.

4. Results

4.1. Application to the description of the behavior of Zirconium

Kaschner and Gray [37], Tomé et al. [12] and Kaschner et al. [13] have reported results of an experimental study on the anisotropy of deformation of textured polycrystalline pure zirconium. This material is highly anisotropic both at the single-crystal and polycrystal level. It was processed through a series of clock-rolling and annealing cycles to produce a plate with strong basal texture ($\langle c \rangle$ -axes of the crystals predominantly oriented along the plate normal direction). The process of multiple rolling passes with rotation was used in order to obtain a nearly isotropic in-plane texture. Right-circular cylindrical tests specimens were sectioned from both the through-thickness (TT) and in-plane (IP) plate directions. Quasi-static compression tests were conducted on these samples (denoted as TTC and IPC), while quasi-static tension tests were conducted only in the IP direction (IPT). The experimental tests have shown that the mechanical response is strongly dependent on the predominant orientation of the $\langle c \rangle$ -axes with respect to the loading direction. While the experiments reported in Refs. [12,13] correspond to two different temperatures (room and liquid nitrogen), in what follows we will use only the room temperature results to validate the proposed model. For the identification of the anisotropy coefficients involved in the CPB05 expressions (see Eq. (15)), the yield stresses corresponding to at least another two different strain paths besides TTC, IPC and IPT are necessary. To obtain the yield stresses for through-thickness tension and shear in different directions, we have performed numerical tests with the VPSC polycrystal model using the reported initial texture (consisting of 377 orientations), deformation mechanisms operational at room temperature (i.e. prismatic $\langle a \rangle$ -slip, pyramidal $\langle c + a \rangle$ -slip and tensile twinning) and the values for the slip system parameters (critical stresses, hardening coefficients, rate sensitivity exponent); see Refs. [12,13]. Using the yield stress data from mechanical tests and the results of the numerical tests by least squares we have fitted the CPB05 yield surfaces (i.e. the nine independent coefficients of the fourth-order tensor \mathbf{L} and the strength-differential parameter k) for five different individual levels of accumulated plastic strain: $\tilde{\epsilon}_p^1 = 0.0002$, $\tilde{\epsilon}_p^2 = 0.01$, $\tilde{\epsilon}_p^3 = 0.05$, $\tilde{\epsilon}_p^4 = 0.1$ and $\tilde{\epsilon}_p^5 = 0.15$. The numerical

Table 1

Yield criterion coefficients corresponding to Fig. 1

	0.2%	1%	5%	10%	15%
k	-0.0017	0.2756	-0.1621	-0.1659	-0.1828
L_{12}	3.7403	2.7390	3.2358	3.2749	3.1351
L_{13}	2.1468	2.0252	1.6811	1.6275	1.6353
L_{22}	0.9926	0.9413	0.8142	0.6188	0.72011
L_{23}	2.0845	1.9900	1.5974	1.5191	1.5212
L_{33}	0.5393	1.2506	1.3113	1.3190	1.1806
L_{44}	1.2958	0.4906	0.6567	0.7695	0.7549
L_{55}	1.4085	0.5560	0.6290	0.7021	0.6858
L_{66}	5.1832	1.9010	2.7404	3.0585	2.9195

For all levels of effective plastic strain: $a = 2$ and $L_{11} = 1.0$.

values for the coefficients for each level of accumulated plastic strain are given in Table 1. It is worth noting that the homogeneity parameter was considered to have a fixed value $a = 2$, because of the nearly elliptical shape of the yield loci for high-purity zirconium. Next, for each individual strain level $\tilde{\epsilon}_p^j$, $j = 1, \dots, 5$, we calculated $Y^j = Y(\tilde{\epsilon}_p^j)$ using the experimental IPT loading curve, and $\tilde{\sigma}^j = \tilde{\sigma}\{\sigma, \mathbf{L}(\tilde{\epsilon}_p^j), k(\tilde{\epsilon}_p^j), a(\tilde{\epsilon}_p^j)\}$ using Eq. (15). Finally, the yield surface corresponding to any given level of accumulated plastic deformation (between 0 and 0.15) was obtained using the interpolation technique described in Section 3.2. Fig. 1 shows the biaxial plane (σ_{xx}, σ_{yy}) projections of the five individual yield surfaces (solid lines) given by Eq. (13), the available experimental and numerical test results as well as several yield loci (dashed lines) obtained

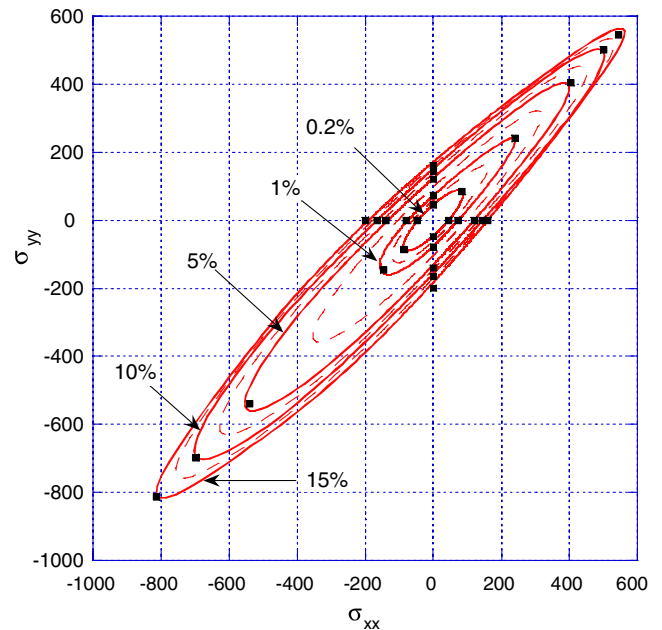


Fig. 1. Yield surface evolution for an initial textured zirconium clock-rolled plate. The solid lines represent the anisotropic CPB05 yield surfaces at individual levels of equivalent plastic strains; the symbols represent the data points used for the determination of the coefficients involved in the analytic yield criterion (experimental measurements as well as flow stresses calculated using VPSC); the dashed surfaces are CPB05 yield surfaces obtained by linear interpolation.

using the proposed interpolation technique (see Eqs. (18)–(21)).

FE calculations were carried out using the above interpolation model to simulate the response of zirconium at room temperature, for the cases of IPT, IPC and TTC. For comparison purposes, we have also performed simulations for the same material assuming fixed values of the anisotropy coefficients (these values correspond to yield stress data at 0.002 equivalent plastic strain) and isotropic hardening. Fig. 2 shows the stress–strain curves obtained using the proposed model (i.e. CPB05 coupled with VPSC using experimentally adjusted anisotropic hardening law), together with those obtained by means of CPB05 but assuming isotropic hardening, and the data from mechanical tests (symbols) [12,38]. Note that the proposed model captures well the experimental trends. Obviously, since isotropic hardening implies that the material hardens at the same rate in every testing direction, it cannot adequately describe deformation that involves the activation of deformation mechanisms different from the ones operational during in-plane tension (i.e. the test used to adjust the values of $Y^j = Y(\bar{\sigma}_p^j)$).

4.2. Simulations of beam bending

The proposed model will be used to simulate a series of four-point bending tests at room temperature reported in Refs. [12,13]. The experiments were carried out on rectangular bars of square section cut from the same clock-rolled Zr. Before loading, the beams were aligned in one of the two possible orientations with respect to the main texture component: with $\langle c \rangle$ -axes mostly aligned with the z -axis of the beam (case C0) and with $\langle c \rangle$ -axes mostly aligned with the x -axis of the beam (case C90) (see also Fig. 3 for a schematic of the test).

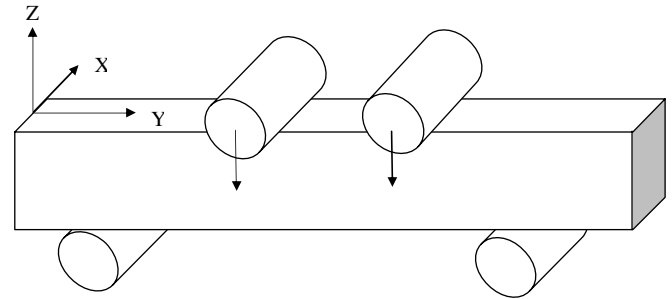


Fig. 3. Schematic of the four-point bend test.

The initial dimensions of the beams were 6.35 mm × 6.35 mm × 50.8 mm. The beams were bent as the upper dowel pins were displaced downwards by 6 mm and the lower pins were held rigid, resulting in a strain of about 20% in the outmost fibers of the beam. Special experimental techniques were developed to map and measure the local strain field (see Refs. [12,13]). Detailed information concerning the variation of each strain component as a function of the location along the width of the specimen was reported for the compressive side (top) as well as the tensile side (bottom). Refs. [12,13] also contain a detailed FE analysis of the bending tests using the explicit FE code EPIC coupled with VPSC (designated VPSC/EPIC in what follows) which was performed assuming the presence of a polycrystal at each integration point. The mesh consisted of 1920 single-integration-point tetrahedral brick elements (the only elements available in EPIC) with the tetrahedra symmetrically arranged in set of 24. For comparison purposes, we implemented the proposed model in EPIC (CPB05/EPIC in what follows) and simulated the same experiments using the same type of elements and the same mesh as in Ref. [12]. Finally, we have also used the present

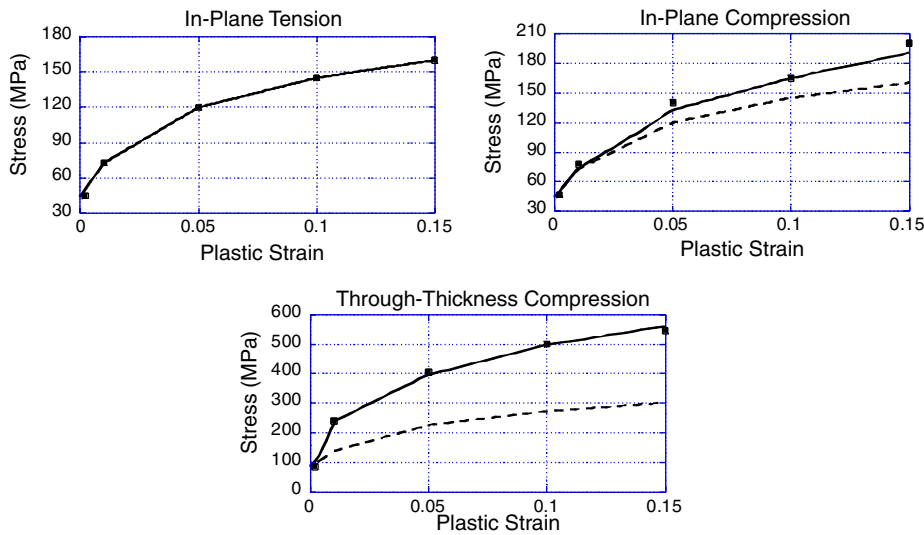


Fig. 2. Comparison between experimental data (solid rectangles) and simulation results using the yield criterion CPB05 with anisotropic coefficients evolving during plastic deformation and CPB05 with fixed anisotropy coefficients (obtained from the initial texture) (dashed lines) for a clock-rolled zirconium plate. Data after Ref. [12]. Error bars are smaller than symbol size (i.e. relative errors in stress and strain measurements are less than 1% and 0.1%, respectively [38]).

model in combination with the explicit ABAQUS FE code (CPB05/ABAQUS in what follows) to simulate the same zirconium bent beam tests using a 9×9 grid of single-integration-point hexahedral elements (CD8R three-dimensional linear brick elements). Due to the symmetry of the problem, only half of the beam was analyzed using 2916 elements. Free-surface boundary conditions were imposed on the beam except at the nodes that coincide with the contact points of the dowel pins. It is worth noting that the adopted discretization is coarser than the one used in the EPIC calculations (the CPB05/ABAQUS calculations involve a total of 5832 elements for the whole beam while the VPSC/EPIC and the CPB05/EPIC simulations involve a total of 7680 elements). The results from these simulations, along with the experimental data and the VPSC/EPIC predictions reported in Ref. [13], are shown in Fig. 4 (C0 case) and Fig. 5 (C90 case). Inspection of Fig. 4 (C0 case) reveals that the simulation results using either VPSC/EPIC or the proposed model (in combination with EPIC or ABAQUS) are reasonably close to the experimental data. Both models capture very well the rigidity of the beam response along the hard-to-deform $\langle c \rangle$ -axes preferential orientation, which in this case is parallel to the z -axis. Also, both models capture the asymmetry between tension and compression (i.e. the differences in yield values

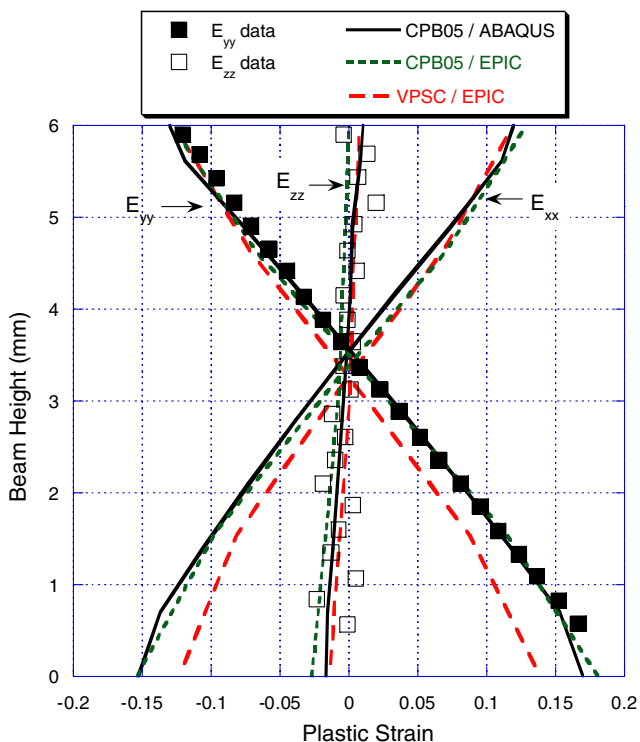


Fig. 4. Comparison of the experimentally measured strain distributions (symbols) with the results of FE simulations using the proposed model implemented in ABAQUS (solid lines), the proposed model implemented in EPIC (interrupted lines) and VPSC linked directly to EPIC (dashed lines), for the case C0 (i.e. when the $\langle c \rangle$ -axes are predominantly contained in the bending plane). Data and VPSC/EPIC simulations results reported in Fig. 6 of Ref. [13]. Data horizontal error bars are roughly equal to symbol size (see Fig. 5 of Ref. [13]).

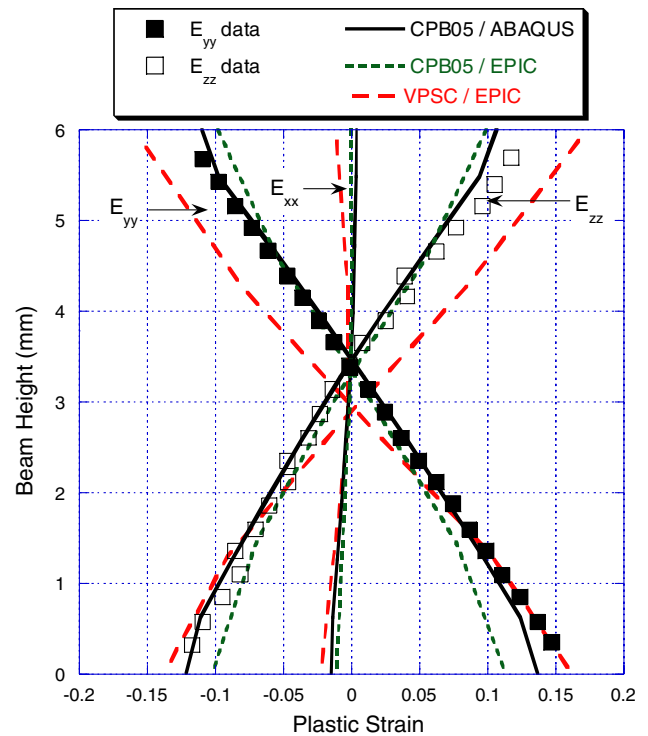


Fig. 5. Comparison of the experimentally measured strain distributions (symbols) with the results of FE simulations using the proposed model implemented in ABAQUS (solid lines), the proposed model implemented in EPIC (interrupted lines) and VPSC linked directly to EPIC (dashed lines), for the case C90 (i.e. when the $\langle c \rangle$ -axes are predominantly perpendicular to the bending plane). Data and VPSC/EPIC simulations results reported in Fig. 6 of Ref. [13]. Data horizontal error bars are roughly equal to symbol size (see Fig. 5 of Ref. [13]).

and hardening rates) and thus correctly predict the shift of the neutral plane. The deformation along the beam axis is better predicted by the proposed model, while the VPSC/EPIC model underpredicts the deformation in the lower half of the beam. Also, the proposed model gives an accurate prediction of upward shift of the neutral plane.

For the case when the major texture component is aligned with the x -axis of the beam (C90, Fig. 5), the CPB05/EPIC calculations underpredict the strains for the lower part of the beam while the upward shift of the neutral axis is reproduced correctly. On the other hand, CPB05/ABAQUS results are much closer to the experimental results. Both the strain distribution and shift of the neutral axis are predicted with accuracy. The better overall performance of the CPB05/ABAQUS implementation compared with the EPIC simulations can be attributed to the use of hexahedral elements (e.g. see Ref. [39]). This may be also the reason why VPSC/EPIC overpredicts the strains for the upper half of the beam but gives a good agreement with the experimental data for the lower half of the beam. However, the predicted VPSC/EPIC neutral plane remains at the center of the beam.

Figs. 6 and 7 present the strain distributions obtained with CPB05/ABAQUS corresponding to the cases C0 and C90, respectively, for the case when the anisotropy

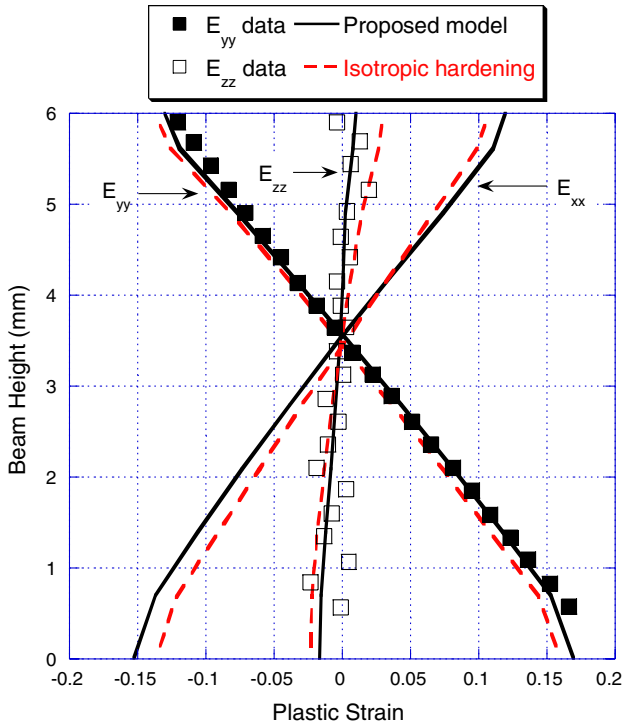


Fig. 6. Comparison of the experimentally measured plastic strain distributions (symbols) and the ABAQUS FE predictions using the proposed model (solid lines) and the CPB05 yield criterion with isotropic hardening (dashed lines) for the C0 case. Data reported in Fig. 6 of Ref. [13]. Data horizontal error bars are roughly equal to symbol size (see Fig. 5 of Ref. [13]).

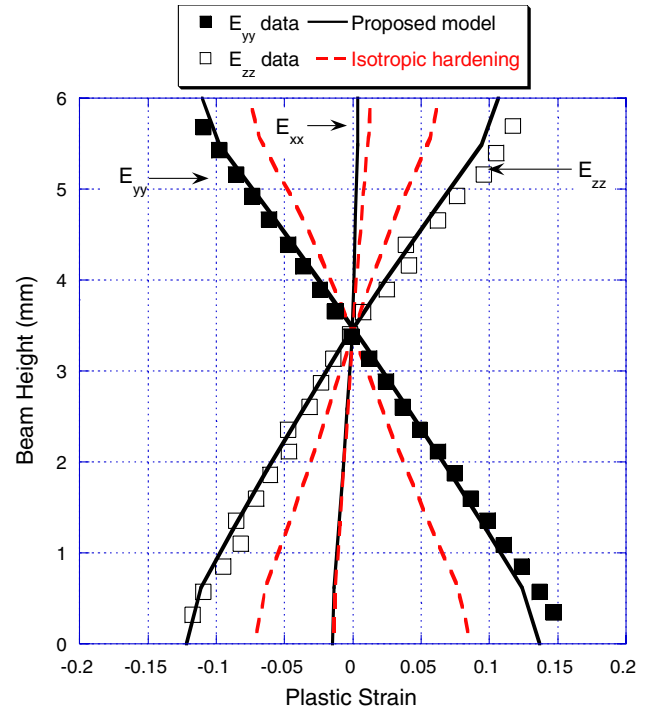


Fig. 7. Comparison of the experimental plastic strain distributions (symbols) and the ABAQUS FE predictions using the proposed model (solid lines) and the CPB05 yield criterion with isotropic hardening (dashed lines) for the C90 case. Data reported in Fig. 6 of Ref. [13]. Data horizontal error bars are roughly equal to symbol size (see Fig. 5 of Ref. [13]).

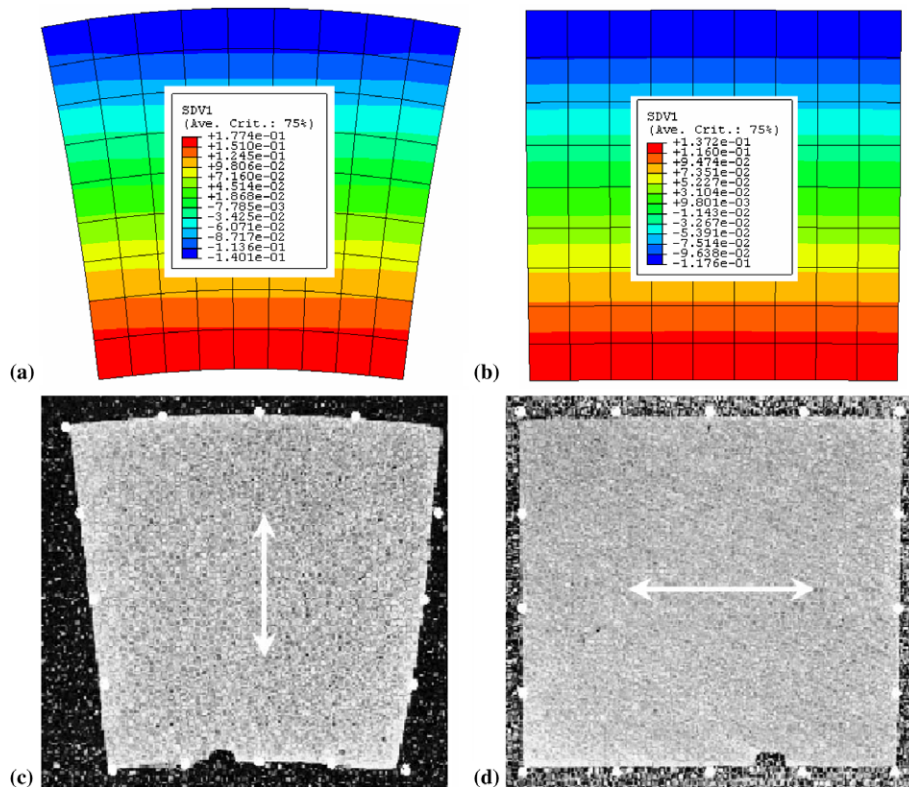


Fig. 8. Comparison of experimentally photographed x - z cross-section of the bent bars versus the predictions of VPSC/EPIC (white dots) and the proposed model (CPB05/ABAQUS implementation). E_{xx} contours corresponding to (a, c) C0 case ($\langle c \rangle$ -axes mostly parallel to the z -axis) and (b, d) C90 case ($\langle c \rangle$ -axes mostly aligned with the x -axis of the beam). The orientation of the basal poles is indicated by the arrows (data and VPSC/EPIC simulations after Ref. [13]).

coefficients are fixed (values of the coefficients were obtained by fitting the yield stress data at 0.002 equivalent plastic strain). Note that CPB05 in conjunction with isotropic hardening reproduces qualitatively well the upward shift of the neutral axis. This is due to the fact that CPB05 incorporates strength-differential effects. However, keeping the anisotropy coefficients constant, i.e. assuming that the shape of the yield locus is given by the initial texture and does not evolve during plastic deformation, we cannot capture the difference in hardening rate between uniaxial tension and uniaxial compression (see also Fig. 2), so the strains distributions are not reproduced quantitatively. In conclusion, excellent agreement between the measured neutral axis displacement and measured strains can be obtained only if the shape of the yield locus is allowed to evolve, i.e. if the difference in hardening rates between in-plane tension and in-plane compression is accounted for.

In what concerns the predictions of the cross-sections of the deformed bars, VPSC/EPIC, CPB05/EPIC and CPB05/ABAQUS models are in agreement with the experimental data. Fig. 8 shows the final configurations for the photographed experimental x - z cross-section of the bent beams superimposed to the predictions obtained with VPSC/EPIC (white dots), as reported in Ref. [13]. The figure also shows the calculated x - z cross-sections of the bent beams obtained with CPB05/ABAQUS (Figs. 8(a) and (b)). Note that both models predict wedged cross-sections for the case C0 (Figs. 8(a) and (c)) when the hard-to-deform $\langle c \rangle$ -axes are predominantly parallel to the z -axis. The wedge-shaped section results from a nearly uniaxial stress loading along the beam axis (the y -axis) that reverses sign at the neutral plane, and from the plastic incompressibility of the material.

For the case C90, when the $\langle c \rangle$ -axes are aligned with the x -axis, VPSC/EPIC and both CPB05/FEM implementations describe correctly the rigidity in the hard-to-deform direction, and predict that the final cross-section remains rectangular, in agreement with the experimentally measured ones. It is worth noting that, as shown in Ref. [12], if a Taylor model (instead of a self-consistent formulation) is used to describe the material response, then the predicted final beam section adopts a wedge shape, contrary to the experimental evidence.

5. Summary and concluding remarks

A macroscopic anisotropic model that captures the influence of evolving texture on the plastic response of hexagonal metals was proposed. Initial yielding is described using a recently developed analytical yield function that accounts for both anisotropy and strength differential effects. To describe the change of the shape of the yield surface during monotonic loading, the evolution of the anisotropic coefficients involved in the expression of the yield function is considered. The evolution laws for the anisotropic coefficients are obtained based on experimental data,

VPSC crystal plasticity theory, together with a macroscopic-scale interpolation technique. A procedure for identification of the parameters involved in the model using flow stress data for simple monotonic single loading paths, in-plane tension, in-plane compression, through-thickness tension, through-thickness compression and pure shear was provided. It was shown that if experimental information is not available or cannot be obtained (e.g. for through-thickness tension or shear loadings), then flow stress data can be generated using the polycrystal calculation in conjunction with the metallurgical information (initial texture, active deformation modes, macroscopic loading curves for simple monotonic single loading paths).

The proposed model was applied to the description of the quasi-static behavior of a high-purity zirconium at room temperature (data reported in Refs. [12,13,37]). The model was benchmarked against beam bending test results. The reason for choosing the bending test is because it provides non-homogeneous forming conditions with deformation gradients and local variables amenable to detailed analysis of the twinning contribution to deformation. Comparison between predicted and measured macroscopic strain fields and beam sections shows that the proposed model describes very well strength differential effects. The difference in response between the tensile and compressive fibers and the shift of the neutral plane are particularly well captured.

Because of non-negligible twinning activity accompanied by grain reorientation and highly directional grain interactions, the influence of the texture evolution on hardening of hcp materials cannot be neglected even for the simplest single loading paths. The model presented is a first attempt to address this very difficult and challenging topic. The simulation results suggest that a computationally efficient macroscale model that incorporates relevant information about the behavior of hcp metals at different length scales describes with high fidelity the quasi-static deformation of initially textured hcp materials for single path loadings.

Acknowledgments

O.C. wishes to thank Dr. Jeong Whan Yoon of Alcoa Inc. for advice and helpful comments related to the finite element implementation of the model. Partial financial support for this work from NSF through Grant DMI-0322730 is gratefully acknowledged. Data in Figs. 2, 6 and 7 were reprinted from Acta Materialia, Vol. 49, Kaschner GC, Bingert JF, Liu C, Lovato ML, Maudlin PJ, Stout MG, Tomé CN, Mechanical response of zirconium – II. Experimental and finite element analysis of bent beams, pp. 3097–3108, Copyright (2001), with permission from Elsevier.

References

- [1] Yoon JW, Barlat F, Dick RE, Chung K, Kang TJ. Int J Plasticity 2004;20:495.

- [2] Prager W. *J Appl Mech* 1956;23:493.
- [3] Ziegler H. *Quart Appl Math* 1959;17:55.
- [4] Chaboche JL. *Int J Plasticity* 1986;2:149.
- [5] Khan A, Huang SH. *Continuum theory of plasticity*. New York (NY): Wiley; 1995.
- [6] Kurtyka T, Zyczkowski M. *Int J Plasticity* 1996;12:191.
- [7] Dawson P. In: Raabe D, Roters F, Barlat F, Chen L-Q, editors. *Continuum scale simulations of engineering materials: fundamentals, microstructures, process applications*. Weinheim: Wiley-VCH; 2004. p. 115.
- [8] Tomé CN, Lebensohn RA. In: Raabe D, Roters F, Barlat F, Chen L-Q, editors. *Continuum scale simulations of engineering materials: fundamentals, microstructures, process applications*. Weinheim: Wiley-VCH; 2004. p. 352.
- [9] Myagchilov S, Dawson PR. *Mater Sci Eng A* 1999;7:975.
- [10] Staroselsky A, Anand L. *Int J Plasticity* 2003;19:1843.
- [11] Salem AA, Kalidindi SR, Semiatin SL. *Acta Mater* 2005;53:3495.
- [12] Tomé CN, Maudlin PJ, Lebensohn RA, Kaschner GC. *Acta Mater* 2001;49:3085.
- [13] Kaschner GC, Bingert JF, Liu C, Lovato ML, Maudlin PJ, Stout MG, et al. *Acta Mater* 2001;49:3097.
- [14] Arminjon M, Bacroix B, Imbault D, Raphanel JL. *Acta Mech* 1994;107:33.
- [15] Van Houtte P, Van Bael A. *Int J Plasticity* 2004;20:1505.
- [16] Van Bael A. PhD thesis, Katolieke University, Leuven, Belgium; 1994.
- [17] Teodosiu C, Hu Z. In: Shen SF, Dawson PR, editors. *Simulations of materials processing theory, methods and applications*. Rotterdam: Balkema; 1995. p. 173.
- [18] Li S, Hoferlin E, Van Bael A, Van Houtte P, Teodosiu C. *Int J Plasticity* 2003;19:647.
- [19] Barlat F, Brem JC, Yoon JW, Chung K, Dick RE, Lege DJ, et al. *Int J Plasticity* 2003;19:1297.
- [20] Cazacu O, Barlat F. *Int J Eng Sci* 2003;41:1367.
- [21] Barlat F, Cazacu O, Zyczkowski M, Banabic D, Yoon JW. In: Raabe D, Roters F, Barlat F, Chen L-Q, editors. *Continuum scale simulations of engineering materials: fundamentals, microstructures, process applications*. Weinheim: Wiley-VCH; 2004. p. 145.
- [22] Bron F, Besson J. *Int J Plasticity* 2004;20:937.
- [23] Barlat F, Aretz H, Yoon JW, Karabin ME, Brem JC, Dick RE. *Int J Plasticity* 2005;21:1009.
- [24] Hill R. *Mathematical theory of plasticity*. Cambridge: Cambridge University Press; 1948.
- [25] Takuda H, Yoshii T, Hatta N. *J Mater Process Technol* 1999;89-90:135.
- [26] Kuwabara T, Katami C, Kikuchi M, Shindo T, Ohwue T. In: *Proceedings of the 7th international conference on numerical methods in industrial forming processes*, Toyohashi, Japan, 18–20 June; 2001. p. 781.
- [27] Cazacu O, Barlat F. *Int J Plasticity* 2004;20:2027.
- [28] Cazacu O, Plunkett B, Barlat F. *Int J Plasticity* 2006;22:1171.
- [29] Kelley EW, Hosford WF. *Trans TMS-AIME* 1968;242:654.
- [30] Lebensohn RA, Tomé CN. *Acta Metall Mater* 1993;41:2611.
- [31] Tomé CN, Lebensohn RA, Kocks UF. *Acta Mater* 1991;39:2667.
- [32] Lee D, Backofen WA. *TMS-AIME* 1966;236:1077.
- [33] Hill R. *J Mech Phys Solids* 1987;35:23.
- [34] ABAQUS Version 6.4 reference manuals, Pawtucket (RI); 2003.
- [35] Belytschko T, Liu WK, Moran M. *Nonlinear finite elements for continua and structures*. New York (NY): Wiley; 2000.
- [36] Simo JC, Hughes TJR. *Computational inelasticity*. New York (NY): Springer; 1998.
- [37] Kaschner GC, Gray GT. *Metall Trans A* 2000;31:1997.
- [38] Kaschner GC. Private communication.
- [39] Cook RD, Malkus DS, Plesha ME, Witt RJ. *Concepts and applications of finite element analysis*. New York (NY): Wiley; 2001.